Organic Electronics 108 (2022) 106570

Contents lists available at ScienceDirect

Organic Electronics

journal homepage: www.elsevier.com/locate/orgel

Pinpointing the origin of the increased driving voltage during prolonged operation in a phosphorescent OLED based on an exciplex host

Markus Regnat [a,b,*], Chang-Ki Moon [c], Sandra Jenatsch [b], Beat Ruhstaller [a,b], Kurt P. Pernstich [b]

[a] Institute of Computational Physics, Zurich University of Applied Sciences ZHAW, 8401, Winterthur, Switzerland
[b] Fluxim AG, Katharina-Sulzer-Platz 2, CH-8400, Winterthur, Switzerland
[c] Research Institute of Advanced Materials (RIAM), Seoul National University, 1 Gwanak-ro, Gwanak-gu, Seoul, 08826, Republic of Korea

ARTICLE INFO

Keywords:
OLED modeling
Simulation
Power efficiency
Degradation
Sensitivity analysis
Trap states

ABSTRACT

We report on the origin of the reduced power efficiency in a red phosphorescent OLED with an exciplex host after prolonged operation. The power efficiency is reduced solely by an increased driving voltage while the radiant flux remains constant. An electrical model describing the driving voltage increase is, thus, sufficient to explain the reduced power efficiency. The electrical model of the fresh OLED and at different stages of degradation was devised from four different measurement methods. Using multiple measurement methods to determine the model parameters results in a rather unique set of model parameters, despite the large number of model parameters (38) as revealed by a correlation analysis. The increase in driving voltage could be reproduced by modifying only 7 out of the 38 model parameters. A sensitivity analysis identified the parameters with the largest effect (66%) on the driving voltage increase to be the trap density and the mobility of the employed hole transporting layer.

This work highlights the benefit of using multiple measurement methods to derive reliable model parameters and the use of a sensitivity analysis to pinpoint the origin of the investigated property.

1. Introduction

Modern displays often employ organic light emitting diodes (OLEDs) as they offer superior picture quality with reduced power consumption compared to conventional display technologies [1,2]. Besides a long operational lifetime and a high external quantum efficiency, an equally important key figure of OLEDs is the power efficiency (PE), which is defined as the ratio of the radiant flux to input power [3]. To achieve a high PE, a low driving voltage together with a high quantum efficiency is required.

Many degradation studies focused on photoluminescence quantum yield and different excitonic effects to explain the reduced radiant flux that leads to a reduced PE after prolonged operation [4–15]. While some of these studies do report on a driving voltage increase [7,11,12], only few studies focused on the origin of the driving voltage increase during prolonged operation [16–20].

As shown in this study, the effect of the driving voltage increase can dominate the degradation over extended periods, thus it is important to better understand this degradation pathway. In the high efficiency OLED reported on in this study, the PE is reduced by an increase of the driving voltage without a reduction of the radiant flux. This enables the detailed analysis of the mechanisms responsible for the degraded performance without having to consider excitonic effects.

In this study, the OLED was operated at constant current for 2800 h and stressing was repeatedly interrupted to obtain the detailed OLED characteristics from four measurement methods. Using multiple measurement methods is necessary to derive a reliable numerical model [21]. Despite its many parameters, the model is very reliable and shows only few correlations between model parameters. The presented electrical model of the fresh and the degrading OLED identifies seven material parameters that change during prolonged operation. A sensitivity analysis of these seven parameters singles out the main cause of the driving voltage increase to be an increased trap density in the employed hole transporting layer. By replacing this layer with a stable, but otherwise identical material, 66% of the driving voltage increase could be avoided and the PE after 2800 h would remain at 92% of its original value.

This work shows how different measurement methods can be used to derive a reliable model, and that a sensitivity analysis helps to single out those parameters, that cause the changes of the investigated property.

* Corresponding author. Institute of Computational Physics, Zurich University of Applied Sciences ZHAW, 8401, Winterthur, Switzerland.
E-mail address: markus.regnat@zhaw.ch (M. Regnat).

https://doi.org/10.1016/j.orgel.2022.106570
Received 3 February 2022; Received in revised form 24 May 2022; Accepted 28 May 2022
Available online 3 June 2022

2. Experimental

The OLEDs were fabricated as described in Lee et al. [22] by thermal evaporation in a vacuum of 5×10^{-7} torr and encapsulated with a glass lid including a moisture getter under nitrogen atmosphere. The samples were shipped, and measurements commenced approx. 2 weeks after device fabrication. The OLEDs were operated for 2800 h at a constant current density of 0.5 mA/cm^2 using a home-built setup under ambient conditions. The current density of 0.5 mA/cm^2 corresponds to an initial luminance of ≈1000 cd/m^2.

To measure a set of four different OLED characteristics, the stressing was briefly interrupted after 663 h, 1456 h, 1756 h and 2799 h. For those intermediate measurements, Fluxim's all-in-one measurement system Paios [23], equipped with a temperature module and a photomultiplier from Hamamatsu (H11526 Series), were used. Unfortunately, there was a problem with the photomultiplier, thus the reported radiant flux values are recorded only up to 1800 h, while the electrical measurements are presented up to 2800 h. The intermediate characterization included the measurement of the current density - voltage curve, charge extraction using a linearly increasing voltage (CELIV) [24,25], capacitance - voltage and impedance at a temperature of 300 K. Maintaining a constant temperature for the intermediate measurements was important, as temperature variations of a few degrees already changed the driving voltage significantly. For the CELIV measurements, an offset voltage was applied for 20 μs before extracting mobile charge carriers with a linear voltage ramp with a slope of 0.2 V/μs to an end voltage of −3 V. The radiant flux was measured in transient electroluminescence experiments as described in Ref. [26]. More details on the different measurement techniques are described in Ref. [27].

The obtained data were analyzed with Fluxim's Characterization Suite software (version 4.3), which included the Setfos-Paios-Integration feature [23] to perform the model parameter optimizations for fitting the measured data as described below.

Current-voltage curves measured at the beginning and the end of the intermediate characterizations showed essentially no changes, indicating that the degradation was solely caused by the prolonged constant current operation.

3. Device model and parameter optimization

To model the electrical characteristics of the bottom-emission phosphorescent exciplex host OLED, the simulation software Setfos (version 4.6) from Fluxim was used [23,28], which calculates position- and time-dependent charge carrier density distributions [29,30]. An exemplary charge carrier distribution for the fresh OLED operated at 0.5 mA/cm^2 is shown in Fig A1.

The highest occupied molecular orbital (HOMO) and lowest unoccupied molecular orbital (LUMO) energy levels together with the layer thicknesses of the OLED stack are shown in Fig. 1. For the indium tin oxide (ITO) anode and the aluminum (Al) cathode, the metal work functions are used and Fermi-level alignment with adjacent layers (ohmic injection) was assumed. For the hole injection layer (HIL) TAPC (4,4′-cyclohexylidenebis[*N*,*N*-bis(4-methylphenyl)benzenamine]) was used, for the hole transporting layer (HTL) NPB ([*N*,*N*′-diphenyl-*N*,*N*′-bis(1,1′-biphenyl)-4,4″-diamine]) and for the electron transport layer (ETL) PO-T2T (triazine [(1,3,5-triazine-2,4,6-triyl)tris-(benzene-3,1-diyl))tris(diphenylphosphine oxide)) were used. The doped ETL (ETL$_{doped}$) was formed by doping PO-T2T with 0.5 wt% Rb_2CO_3 and was modelled by introducing a fixed electron donor density. The exciplex host comprises NPB and PO-T2T in a molar ration of 1:1. Together with 5 wt% of the red emitter Ir(mphmq)$_2$(tmd)(bis(4-methyl-2-(3,5-dimethylphenyl)quinoline))Ir(III)(tetramethylhepta-dionate)), the co-host forms the emission

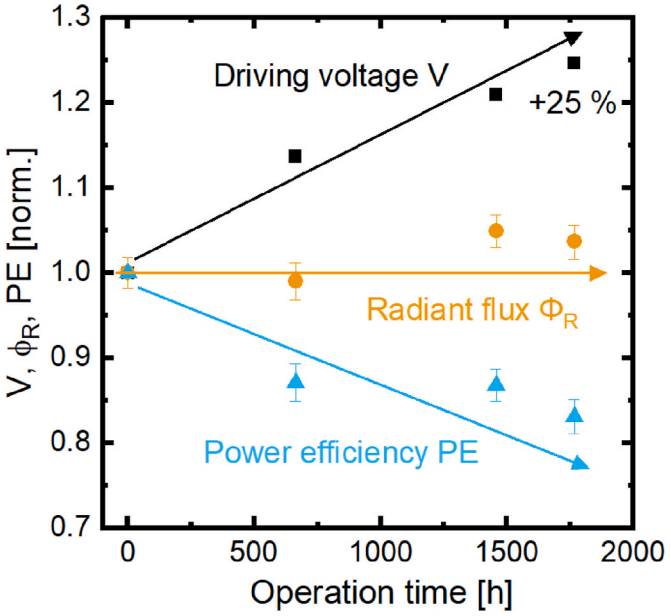

Fig. 2. Driving voltage, radiant flux and power efficiency during constant current operation at 0.5 mA/cm^2 for the first 1800 h. The arrows are guides to the eye.

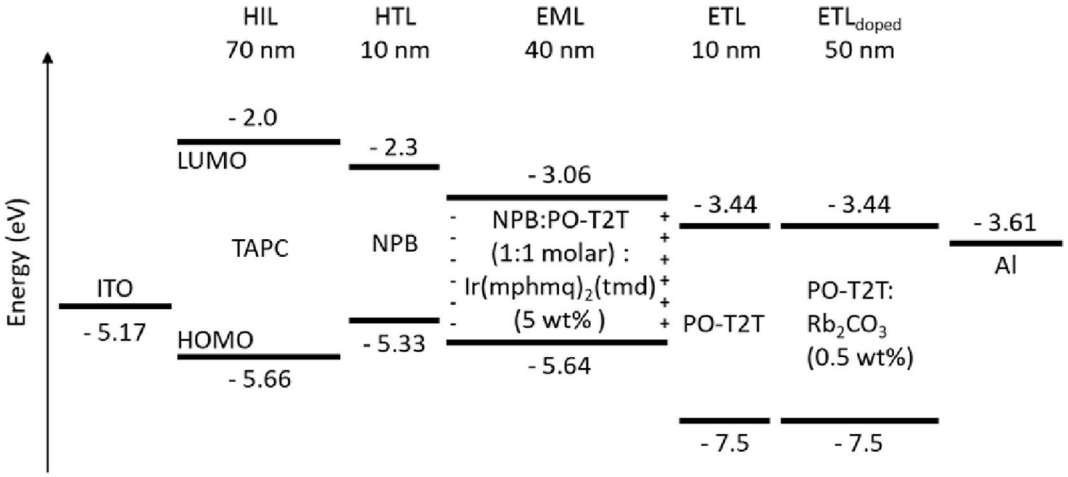

Fig. 1. LUMO/HOMO energy levels and thickness of each layer. For ITO and the Al electrode, the energy level represents the work function. The fixed charge density in the EML (plus and minus signs) accounts for the spontaneous orientation polarization of the EML.

layer (EML). The HOMO and LUMO energy levels of the EML had to be adjusted from the energy levels of the pure NPB and the pure PO-T2T levels, respectively, as discussed previously [31]. The electron and hole mobilities in the exciplex EML were field dependent, while in the transporting layers (HIL, HTL, ETL and ETL_{doped}), only the majority charge carrier mobilities were taken as field dependent (cf. Table 1). As discussed below, the EML is modelled with a fixed charge density in a 2 nm thin layer at both EML sides (plus and minus signs in Fig. 1) [28,29] to account for a spontaneous orientation polarization (SOP) [32] in the EML. It is likely that the SOP in the EML originates from the preferred orientation of the emitter molecules [27] rather than the exciplex host, but the exact origin has no influence on the findings of this study.

The model parameter determination and optimization was performed through the Setfos-Paios-Integration (SPI) feature in Fluxim's Characterization Suite software [23]. The SPI module allows to define a Setfos model in the Characterization Suite, which also controls the measurements, performs the simulations, and compares the results with the measurements inside an optimization or fitting routine. For the optimization we followed the description by Jenatsch et al. [27], where the optimization routine started with an initial guess obtained by manually selecting parameter values, and uses a combination of global and local fit algorithms. The electrical model comprises 38 free parameters (cf. Fig. 4), thus it is challenging to find a unique set of model parameters. To circumvent this problem, we used the result of four different measurement methods as optimization targets (cf. Fig. 3).

As discussed in the context of the correlation analysis below, we argue that this approach leads to a reliable set of model parameters. As an additional verification of the electrical model, optically detuned OLEDs were fabricated to determine the position of the emission zone with an angular emission analysis as described previously [33,34]. The emission zone was predominantly located at the HTL/EML interface, and, in good agreement, an optical model extension of the electrical model also shows a high radiative dipole density at this interface as shown in Figure A2.

Table 1
Model parameters for each layer of the fresh OLED device.

	TAPC	NPB	NPB:PO-T2T	PO-T2T & PO-T2T:Rb_2CO_3
Thickness (nm)	70	10	40	10 & 50
Relative permittivity (−)	3.308	3.373	2.76	3.1
LUMO/HOMO (eV)	−2.0/−5.66	−2.3/-5.33	−3.06/−5.64	−3.44/−7.5
Density of chargeable sites ($1/m^3$)	1e27	1e27	5e26[a]	1e27
Acceptor/donor doping ($1/m^3$)	-/-	-/-	3.79e24/3.79e24[b]	-/2.4e25[c]
Hole/electron				
Zero-field mobility (cm^2/Vs)	8.32e-3/[d]	1.98e-5/[d]	6.71e-6/2.43e-5	[d]/3.05e-4
Field enhancement ($(cm/V)^{0.5}$)	5.81e-3/[d]	2.87e-3/[d]	3.56e-3/6.37e-3	[d]/6.11e-3
Hole/electron				
Trap depth (eV)	0.48/-	0.205/-	0.205/0.24	-/0.24
Trap density ($1/m^3$)	2.36e22/-	1.97e24/-	1.07e24/1.33e24	-/1.01e24
Trap capture rate (cm^3/s)	1e-16/-	7.1e-14/-	6.46e-14/1.06e-17	-/1.07e-17

External circuit parameters obtained from postprocessing the measured data of the fresh OLED: ITO series resistance 55.17 Ω and parasitic parallel resistance 3.65 GΩ outside the active OLED area.

[a] Reduced density of chargeable sites for holes and electrons due to co-evaporated NPB:PO-T2T film.

[b] Just 2 nm at both sides in the NPB:PO-T2T, to account for the spontaneous orientation polarization in the EML. This value translates to a sheet charge density of 1.2 mC/m^2 which is similar to the value reported for Alq3 [35].

[c] Only for PO-T2T:Rb_2CO_3 layer to simulate electrically doped PO-T2T with 0.5 wt% Rb_2CO_3.

[d] For minority charge carriers in the hole or electron transporting layers very low zero-field mobilities of 1e-8 cm^2/Vs without field enhancement were assumed.

4. Results and discussion

Fig. 2 shows the measured driving voltage V and radiant flux Φ_R during prolonged operation for constant current I. No significant change in radiant flux for the first 1800 h of operation was observed, which agrees with a previous study by Lee at al [22]. on the same OLED stack. The error bars on the radiant flux are associated with the uncertainty in interpolating the measurements, as the data points were taken at equidistant voltages and not at 0.5 mA/cm^2. During prolonged operation, the driving voltage V increased from an initial value of 2.75 V by 25%, resulting in a corresponding power efficiency decrease, as the PE is given by $PE = \frac{\Phi_R}{I \cdot V}$. As shown in the following, the electrical model identifies an increased trap density in the TAPC layer as the main cause of the driving voltage increase, thus, explains the reduced PE.

4.1. Fresh OLED

Fig. 3 shows the measured and simulated current density - voltage (JV) curve together with the CELIV measurements, the capacitance - voltage curve and the impedance data of the fresh OLED. The electrical device model nicely reproduces the measurements from the four different methods in the whole frequency-, time- and voltage range. In Fig. 3a, the current density - voltage curves are shown in linear and logarithmic representation. The OLED shows a very low onset voltage of 1.8 V, which is typical for co-host exciplex OLEDs [36–38].

Fig. 3b shows the injection CELIV measurements for three offset voltages. With increasing offset voltage, the peak height increases and shifts to later times. The existence of a peak in injection CELIV at an offset voltage of 1 V, i.e., below the onset voltage of the OLED, indicates the presence of one charge carrier type in the device. One possible reason for such a behavior is the injection and accumulation of carriers due to a polar layer [25,39]. The peak height and its position are sensitively related to the charge carrier dynamics, thus, CELIV measurements are important fit targets for the model parameter optimization. Namely, the integral of the peak is related to the amount of extracted and previously injected charge whereas the peak position is related to the carrier mobility.

Fig. 3c shows the capacitance-voltage measurement where the constant capacitance at negative voltage represents the geometric capacitance of the OLED device. The capacitance peak marks the built-in voltage of ≈1.8 V, where recombination of electron and holes becomes significant. The capacitance rise at negative voltage and the formation of a plateau indicates an enhanced charge carrier injection for one species (holes or electrons) due to the presence of a sheet charge density in the OLED stack, which is in agreement with the observations in the CELIV transient at 1 V. This sheet charge density can, in principle, be caused by either fixed (interface) trap states or a polar layer. We argue that traps are not at work because as discussed in the context of Fig. 5, the onset voltage after prolonged operation shifts towards higher voltages, thus the trap density should be reduced, which is implausible. However, in the presented case, there is evidence for the presence of a polar layer as discussed below, thus it is likely, that the sheet charge density induced by the polar layer causes the measured plateau. The same effect has been shown in Ref. [40] using a similar emitter dopant. In the device model, this polar layer is modelled by introducing thin doped layers in the emission layer at both interfaces (cf. Fig. 1).

Fig. 3d shows the frequency dependent capacitance for four offset voltages. At frequencies below 10^3 Hz, the different capacitance plateaus show the voltage dependent charge carrier accumulation in the transport layers which vanish for higher frequencies. The electrical

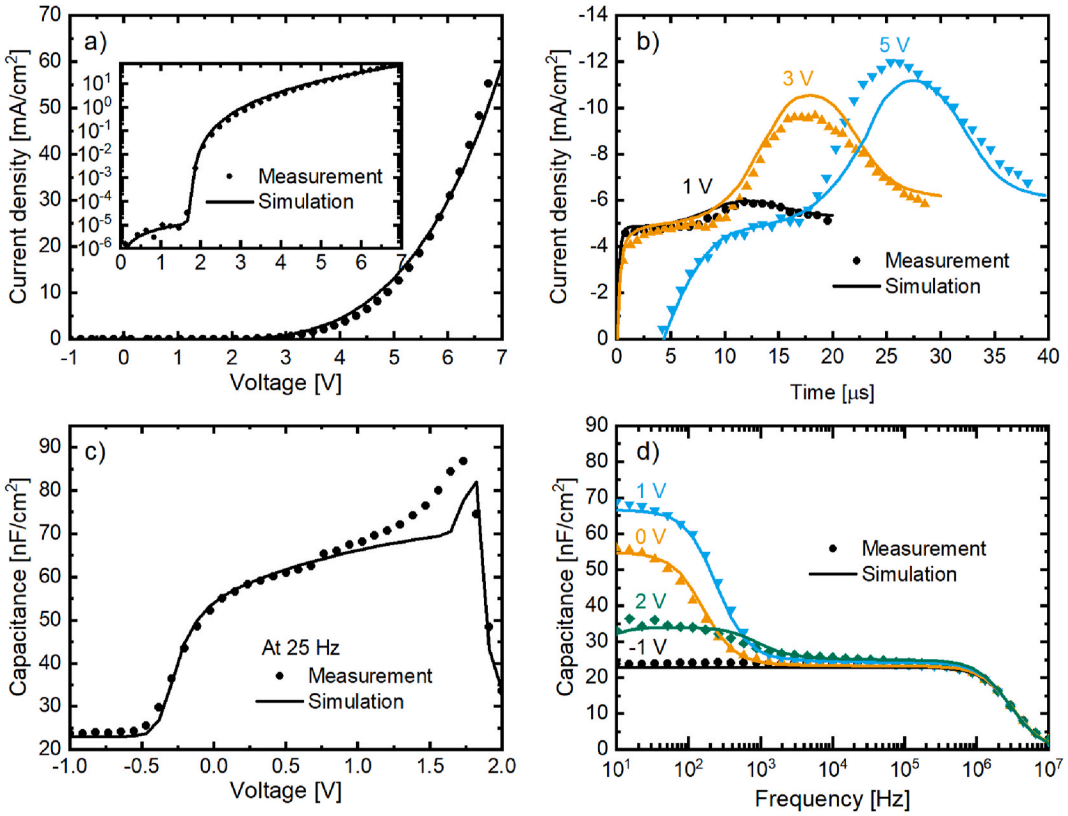

Fig. 3. Measured and simulated current density - voltage curve (a), injection CELIV measurements (b), capacitance - voltage (c) and impedance curves (d) of the fresh OLED, demonstrating the excellent agreement between measurement and simulation.

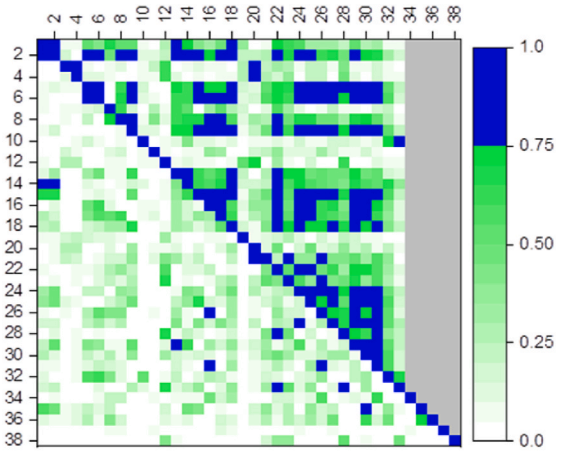

1	TAPC – hole mobility field-enhancement	20	TAPC – relative permittivity
2	TAPC – zero-field hole mobility	21	NPB – relative permittivity
3	NPB – hole mobility field-enhancement	22	EML – relative permittivity
4	NPB – zero-field hole mobility	23	POT2T – relative permittivity
5	EML – hole mobility field-enhancement	24	TAPC – hole trap density
6	EML – zero-field hole mobility	25	NPB – hole trap density
7	EML – electron mobility field-enhancement	26	EML – hole trap density
8	EML – zero-field electron mobility	27	EML – electron trap density
9	EML – acceptor/donor doping	28	POT2T – electron trap density
10	POT2T – electron mobility field-enhancement	29	TAPC – hole trap depth
11	POT2T – zero-field electron mobility	30	NPB – hole trap depth
12	POT2T Rb_2CO_3 – donor doping	31	EML – hole trap depth
13	ITO – work function	32	EML – electron trap depth
14	TAPC – HOMO level	33	POT2T – electron trap depth
15	NPB – HOMO level	34	TAPC – hole trap capture rate
16	EML – HOMO level	35	NPB – hole trap capture rate
17	EML – LUMO level	36	EML – hole trap capture rate
18	POT2T – LUMO level	37	EML – electron trap capture rate
19	Al – work function	38	POT2T – electron trap capture rate

Fig. 4. Correlation matrix of the 33, respectively 38 model parameters allowed to vary during optimization for JV only (upper part) and for all four measurement methods (lower part), where 1 (blue) is fully positively or negatively correlated and 0 (white) is uncorrelated.

model accurately reproduces this transition to higher frequencies, which is important as the degradation changes this transition frequency (c.f. Fig. 5d).

4.2. Correlation analysis

To gain confidence in the device model and the optimized parameter set, the parameter correlation was calculated from the Jacobian matrix of the gradient-based optimizer [21]. The triangular part above the diagonal of the correlation matrix shown in Fig. 4 was calculated when only the JV measurements were considered as optimization target, while the triangular part below the diagonal considered all four measurement types in Fig. 3. Parameter correlation for parameters 34 to 38 (grey area in Fig. 4) could only be calculated for the lower part, as the trap capture rates are not used in the steady state simulations of the JV characteristics. The matrix shows the absolute values of correlations, where a value of 1 stands for fully positively or negatively correlated parameters, and a value of 0 for completely uncorrelated parameters. The lower part shows much less correlation than the upper part, highlighting the advantage of using different measurement types as optimization target to obtain a reliable set of model parameters [21,27].

Fig. 4 highlights correlations >0.75 with blue color, and in the lower

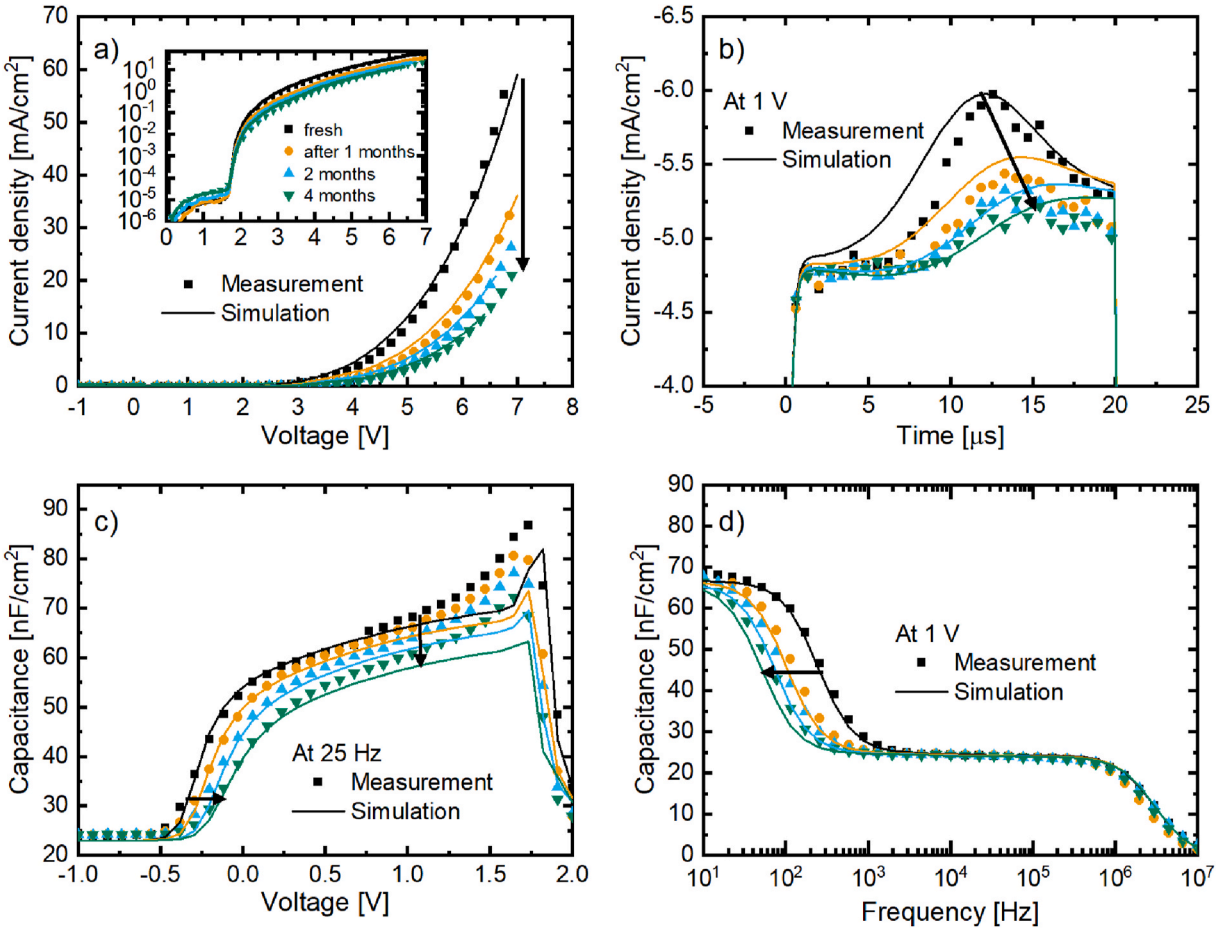

Fig. 5. Measured and simulated JV (a), CELIV (b), *C*–V (c) and impedance (d) curves of the fresh (black) and degraded states after one (orange, 663 h), two (blue, 1456 h) and four months (green, 2799 h) of prolonged constant current operation.

part, only 13 strong correlations exist. Out of these 13 strong correlations, 9 correlations are between zero-field mobility and mobility field-enhancement, between energy levels and mobility parameters, or between trap depth and trap density, trap capture rate or energy levels. Correlations between those parameters are generally encountered in modelling of OLEDs and efforts should be made to directly measure those parameters with independent measurement methods. The device specific correlations between parameters 21/20, 28/22, 33/22 and 27/24 might be coincidental and not significant: apart from parameter 24, none of the other parameters had to be changed to describe the aging of the OLED, thus they appear to have a minor influence on the investigated property, i.e., the driving voltage. A more detailed sensitivity analysis could shed light on the significance of these correlations but goes beyond the scope of this study. Despite the 38 model parameters that were allowed to change during optimization, surprisingly little uncertainty in the model parameters remains if multiple measurement methods are used as optimization target.

4.3. Degraded OLED

Having the quantitative electrical device model for the fresh OLED at hand, selected model parameters are modified to describe the measurements after prolonged operation. From the modified model parameters, the mechanism reducing the PE is inferred. By pinpointing deteriorating material parameters, future developments can be better targeted. For the optimization of the model parameters to describe the measurements after prolonged operation, only the trap density and the mobility parameters of each layer as well as the polarization of the EML (14 parameters) were allowed to evolve with time. Table A1 lists the evolved model parameters after 1, 2 and 4 months. Parameters such as the LUMO/HOMO energy levels, relative permittivity, and trap depth of each layer, as well as the ITO and Al work function and the ETL donor doping were kept unchanged.

Fig. 5 shows the measured and simulated data of the fresh (black) and degraded OLED states after one (orange), two (blue) and four months (green) of constant current stressing. The lines in Fig. 5 show the simulation results, which describe the measurements quite well over the entire time span. Some improvements of the fit quality are discussed below.

The most obvious change after prolonged operation is seen as a reduced current at a given operating voltage in Fig. 5a. Within four months, the current density dropped nearly by a factor of 3 from 55 mA/cm^2 at 6.8 V to 19.1 mA/cm^2.

The injection CELIV peaks in Fig. 5b are reduced and shift to later times indicating a reduced carrier mobility. Corresponding data for offset voltages of 3 V is given in Figure A3. The small deviation of the simulated currents in Fig. 5b at times $> 15\,\mu s$ can be improved by reducing the hole trap capture rate in NPB and EML (cf. Figure A4). We like to note that the default behavior in Setfos also reduces the trap capture rate with increasing trap density according to the theory described in Ref. [41], but this reduction was not sufficient to explain the measurements. The reduced capture rates only improve the quality of the simulated CELIV peaks because it is only required for transient, and not for steady state simulations. Therefore, it does not influence the driving voltage and was, thus, not further considered.

The capacitance-voltage data in Fig. 5c shows that the capacitance onset voltage shifts to higher voltages and the capacitance below the built-in voltage of ≈1.75 V is reduced, while the position of the

capacitance peak at the built-in voltage remains essentially the same.

In the impedance measurements shown in Fig. 5d, the transition frequency shifts to lower frequencies. Corresponding data for offset voltages of −1 V, 0 V and 2 V are given in Figure A5.

With the quantitative model describing the OLED degradation at hand, the influence of the changed model parameters on the driving voltage increase is discussed in the following.

Fig. 6 gives an overview of the model parameters that were modified to reproduce the measured changes during prolonged operation, and Table A1 lists the numeric values.

Fig. 6a shows the evolution of the trap densities in each semiconducting layer. For the transport layers (HIL, HTL, ETL, ETL_{doped}), only traps capturing majority charge carriers were allowed to change, while for the EML, electron and hole traps were free parameters during optimization. The biggest change was observed for the hole trap density in the TAPC layer, which increased by a factor of 9. The hole trap density in the NPB and in the NPB_{EML} increased by a factor of 2 and 1.8, respectively. The increased trap density in TAPC and NPB indicates degradation in those materials, which is consistent with previous reports [42–44]. The larger increase of traps in TAPC than in NPB is likely caused by the lower intrinsic stability of TAPC [42] and not by a high charge carrier density (cf. Fig. A1) nor by excitonic processes as TAPC is farther away from the emission zone as NPB (cf. Fig. 1). Surprisingly, no increase of electron trap density in PO-T2T in the $PO\text{-}T2T_{EML}$ was observed, indicating the stable operation of PO-T2T in the investigated period, which might - at least in part - be explained by the large distance from the emission zone (cf. Fig. A2) [45].

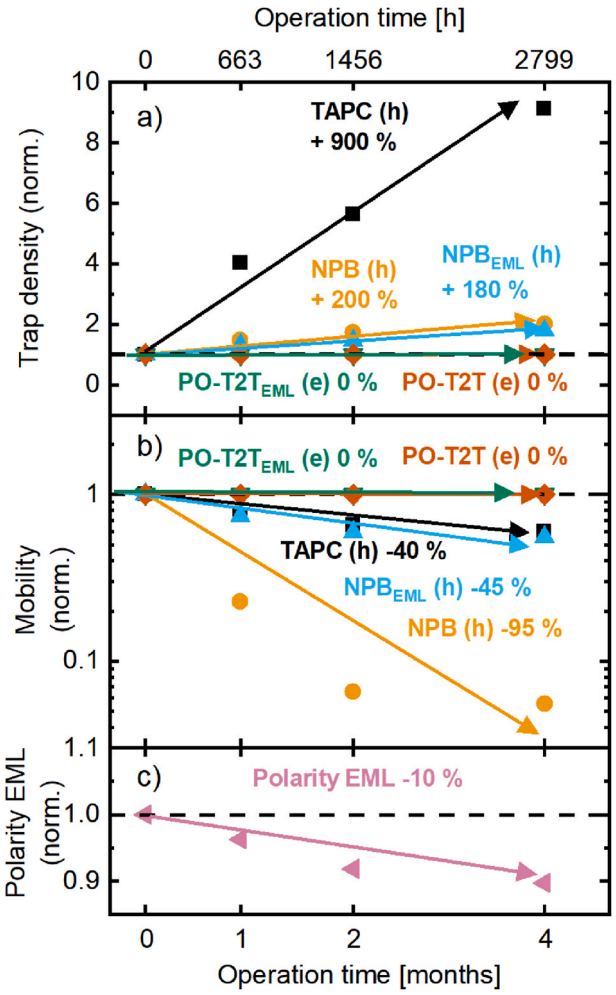

Fig. 6. Changes of the model parameters during prolonged operation. The influence of each parameter on the driving voltage is elucidated in the sensitivity analysis. The arrows are guides to the eye.

Fig. 6b shows the evolution of the zero-field mobilities in each semiconducting layer. As for the trap densities, only the zero-field mobilities of the majority charge carriers were allowed to change in the transporting layers (HIL, HTL, ETL, ETL_{doped}), while for the EML, the electron and hole mobilities were free parameters during optimization. The hole mobility in the TAPC had to be reduced by 40%, which is a similar reduction as in the NPB_{EML} of 45%. The biggest change was a reduced hole mobility in the NPB of 95%. The electron mobilities for the PO-T2T in the EIL and ETL remained unchanged during prolonged operation, again indicating stable operation of the PO-T2T. A comparison of the increased trap densities in Fig. 6a with the reduced mobilities in Fig. 6b suggests that the introduction of trap states reduces the mobility and that the extent to which new trap states reduce the mobility depends on the material, respectively the trap depth as discussed in Refs. [46,47]. We argue that the introduction of trap states does not affect the microscopic mobility, i.e., the hopping rate between adjacent molecules, but rather reduces the effective mobility due to a reduced percolation path or scattering at (charged) trapping site.

The last parameter that had to be changed to quantitatively describe the degradation during prolonged operation was the fixed sheet charge density at both sides of the EML (accounting for the spontaneous orientation polarization), which had to be reduced by 10% as shown in Fig. 6c. This reduction is necessary to accurately describe the shift of the capacitance onset towards more positive voltages in Fig. 5c. The reduced sheet charge density indicates that molecules reorient to a more random orientation in the presence of an electric field during the prolonged operation. A reorientation of molecules in an electrical field has been discussed in Ref. [48].

4.4. Sensitivity analysis

Thus far, the model parameters that influenced all four measurements were discussed. As discussed in the context of the CELIV measurements, not all parameters in Fig. 6 influence the steady state JV characteristics, thus it is important to isolate those model parameters, that do influence the driving voltage in order to draw the right conclusions. This is particularly true when multiple measurement methods are used to determine a reliable set of model parameters.

In the following sensitivity analysis, the influence of the evolved model parameters shown in Table A1 and in Fig. 6 on the driving voltage, respectively the PE (cf. Fig. 2), are investigated.

Fig. 7 shows the driving voltage increase with respect to the fresh OLED when a single parameter (orange bars) of the degraded model after four months was reverted to its value in the fresh OLED (cf. Table A1). Reverting only the trap density in TAPC had the largest effect (53%) on the observed driving voltage increase, followed by reverting only the TAPC zero-field mobility (21%). Thus, if TAPC would be replaced with a stable, but otherwise identical material, 66% of the driving voltage increase (green bar in Fig. 7) could be avoided. In such an OLED, the driving voltage would only increase by 0.224 V and the power efficiency would remain at 92% of its original value after 2800 h continuous operation at 1000 cd/m^2. In comparison, replacing the NPB in the HTL and the EML with an identical but stable material only accounts for 24% of the observed driving voltage increase, and the increased polarity of the EML accounts for 11%.

From this, it seems advisable to replace the TAPC hole transporting material with a more stable material for an improved power efficiency of the OLED during prolonged operations.

5. Conclusion

The investigated red phosphorescent OLED with an exciplex host exhibited an increased driving voltage during prolonged operation at constant current without a reduction in radiant flux, resulting in a

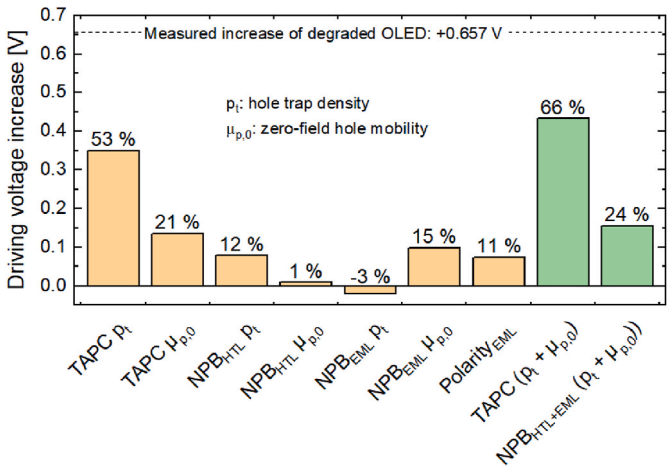

Fig. 7. Sensitivity analysis of the driving voltage increase with respect to the fresh OLED when only a single parameter of the degraded model was reverted to its original value in the fresh OLED (orange columns). By replacing TAPC or NPB hole transporting material (green columns) with a stable but otherwise identical material, 66% respectively 24% of the driving voltage increase could be avoided.

corresponding PE reduction. During prolonged operations, multiple measurement methods were repeatedly applied and used as optimization target to derive a reliable electrical model of the fresh and the degrading OLED. A correlation analysis revealed that despite the large number of model parameters (38), a reliable and rather unique set of model parameters could be found. The evolution of the OLED characteristics during degradation could be reproduced by modifying only seven model parameters. A sensitivity analysis revealed that out of these seven parameters, the hole trap density and the zero-field mobility of the TAPC hole transporting layer had the largest impact on the driving voltage increase, thus on PE. Replacing TAPC with a stable but otherwise identical material would avoid 66% of the driving voltage increase and the PE would remain at 92% of its original value after 2800 h continuous operation. Interestingly, the parameters of the electron transporting material PO-T2T did not change during prolonged operation.

We have shown that using multiple measurement methods results in a reliable model and that a sensitivity analysis helps to pinpoint the parameters which impact the investigated property.

Declaration of competing interest

The authors declare that they have no known competing financial interests or personal relationships that could have appeared to influence the work reported in this paper.

Acknowledgements

The authors thank Professor Jang-Joo Kim from Seoul National University, S. Züfle and B. Blülle from Fluxim AG and J. Dunst from ZHAW for fruitful discussions and valuable comments. Financial support from the Swiss National Science Foundation under grants no. 162230 and 189182 as well as from the Korea−Swiss Innovation Program (2015K1A3A1A14021006) through a National Research Foundation (NRF) grant funded by the Ministry of Science, ICT, and Future Planning (MSIP) is gratefully appreciated.

Appendix

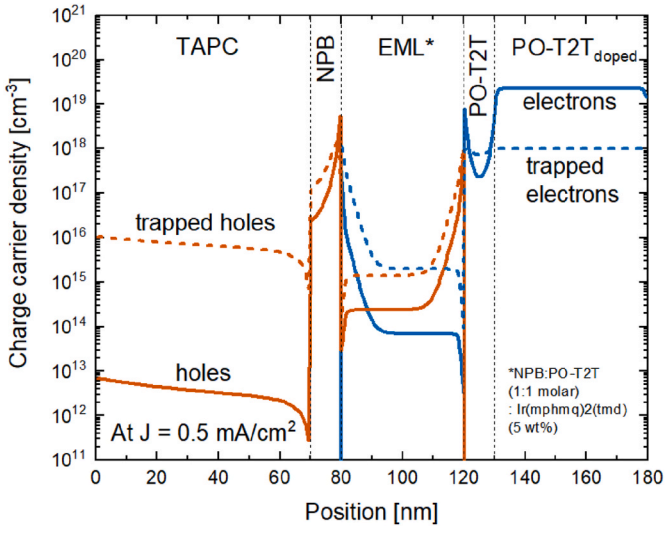

Fig. A1. Distribution of mobile (lines) and trapped (broken lines) hole and electron density in the fresh OLED operated at a current density of $J = 0.5\, mA/\, cm^2$.

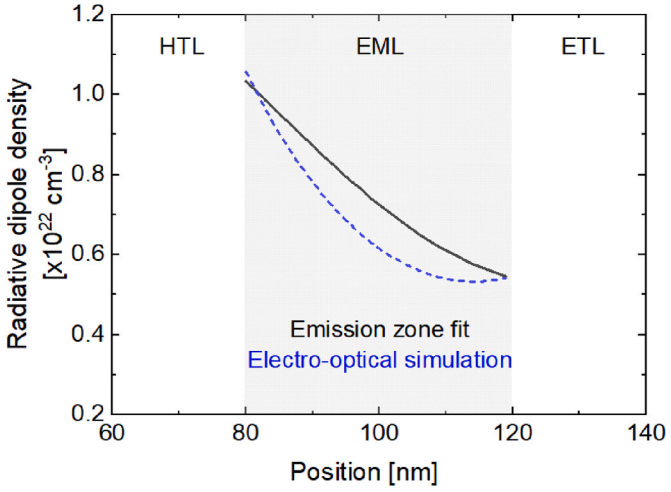

Fig. A2. Comparison of the radiative dipole density determined from an emission zone fit in a detuned OLED (solid line) with electro-optical simulations (dashed line). In the electrical model presented above, only the layer thickness was adapted to that of the detuned OLED to calculate the electron-hole recombination rate. Extending the electrical model with an optical model [29] considering 100% exciton generation, Langevin recombination with a radiative decay rate of 1 us and an exciton diffusion constant of 0.6 nm/ns, the radiating dipole density was calculated. The measured and simulated radiative dipole densities agree well, further verifying the validity of the electrical device model. More details on the emission zone fit can be found in Ref. [33].

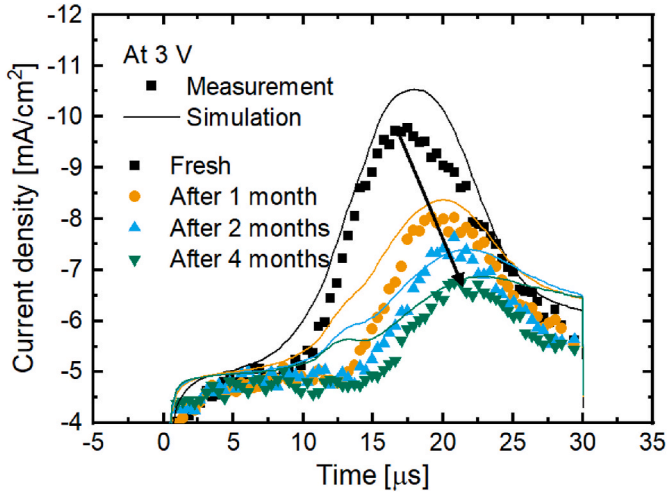

Fig. A3. Measured and simulated CELIV curves of the degraded OLED at an offset voltage of 3 V (cf. Fig. 5b for 1 V).

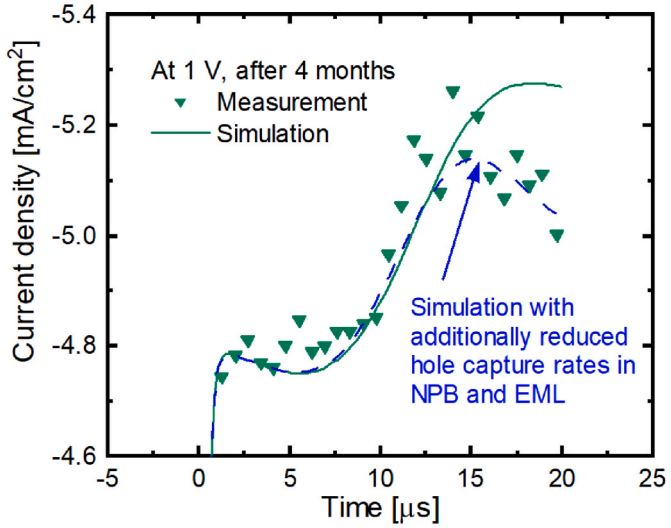

Fig. A4. Improved simulations of the CELIV curve at times >15 μs when the hole trap capture rates in the NPB and EML layers were further reduced (see text for details).

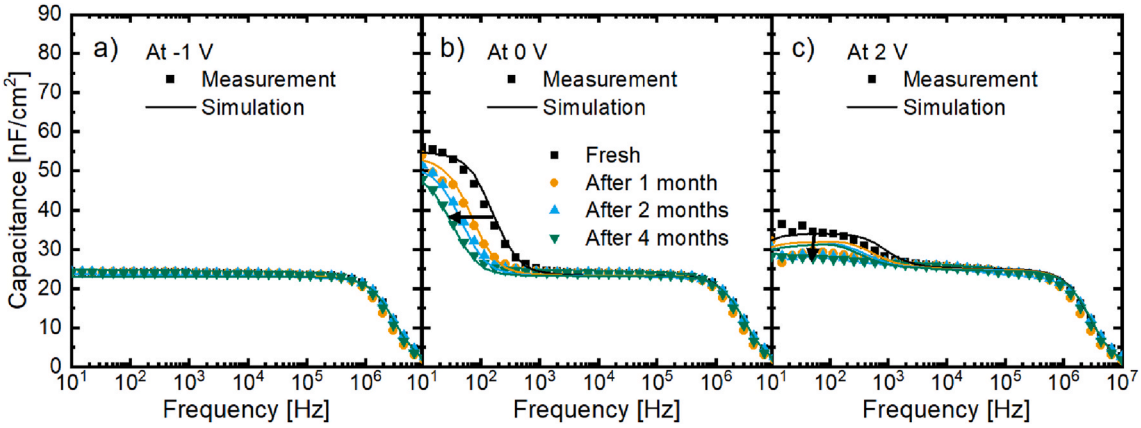

Fig. A5. Measured and simulated impedance measurements at offset voltages of −1, 0, and 2 V (cf. Fig. 5d for 1 V).

Table A1
Model parameters that were changed to describe the degradation.

	Fresh (0 h)	After 1 month (663 h)	After 2 months (1456 h)	After 4 months (2799 h)
TAPC				
Hole trap density ($1/m^3$)	$2.36 \cdot 10^{22}$	$9.5 \cdot 10^{22}$	$1.33 \cdot 10^{23}$	$2.15 \cdot 10^{23}$
Hole zero-field mobility (cm^2/Vs)	$8.32 \cdot 10^{-3}$	$6.22 \cdot 10^{-3}$	$5.44 \cdot 10^{-3}$	$5.01 \cdot 10^{-3}$
NPB_{HTL}				
Hole trap density ($1/m^3$)	$1.97 \cdot 10^{24}$	$2.91 \cdot 10^{24}$	$3.39 \cdot 10^{24}$	$3.95 \cdot 10^{24}$
Hole zero-field mobility (cm^2/Vs)	$1.98 \cdot 10^{-5}$	$4.5 \cdot 10^{-6}$	$1.29 \cdot 10^{-6}$	$1.09 \cdot 10^{-6}$
NPB_{EML}				
Hole trap density ($1/m^3$)	$1.07 \cdot 10^{24}$	$1.41 \cdot 10^{24}$	$1.56 \cdot 10^{24}$	$1.91 \cdot 10^{24}$
Hole zero-field mobility (cm^2/Vs)	$6.71 \cdot 10^{-6}$	$4.99 \cdot 10^{-6}$	$3.98 \cdot 10^{-6}$	$3.72 \cdot 10^{-6}$
EML Polarity				
Acceptor/Donor doping ($1/m^3$)	$3.79 \cdot 10^{24}$	$3.65 \cdot 10^{24}$	$3.48 \cdot 10^{24}$	$3.4 \cdot 10^{24}$

References

[1] V.C. Coffey, The age of OLED displays, Bd. Opt. Photonics News 28 (11) (Nov. 2017) 34–41.

[2] G. Seong, Y. Lee, Y. Kwak, Image quality comparison between LCD and OLED display, Bd. 2021, Electron. Imaging 16 (Jan. 2021), https://doi.org/10.2352/ISSN.2470-1173.2021.16.COLOR-326, 326-1-326–5.

[3] W. Brütting, C. Adachi, Physics of Organic Semiconductors, John Wiley & Sons, 2012.

[4] J.S. Bangsund, K.W. Hershey, R.J. Holmes, Isolating degradation mechanisms in mixed emissive layer organic light-emitting devices, Bd. ACS Appl. Mater. Interfaces 10 (6) (Feb. 2018) 5693–5699, https://doi.org/10.1021/acsami.7b16643.

[5] L.-S. Cui, Y.-L. Deng, D.P.-K. Tsang, Z.-Q. Jiang, Q. Zhang, L.-S. Liao, C. Adachi, Controlling synergistic oxidation processes for efficient and stable blue thermally activated delayed fluorescence devices, Bd. Adv. Mater. 28 (35) (2016) 7620–7625, https://doi.org/10.1002/adma.201602127.

[6] A.S.D. Sandanayaka, T. Matsushima, C. Adachi, Degradation mechanisms of organic light-emitting diodes based on thermally activated delayed fluorescence molecules, Bd. J. Phys. Chem. C 119 (42) (2015) 23845–23851, https://doi.org/10.1021/acs.jpcc.5b07084.

[7] J. Sohn, D. Ko, H. Lee, J. Han, S.-D. Lee, C. Lee, Degradation mechanism of blue thermally activated delayed fluorescent organic light-emitting diodes under electrical stress, Bd. Org. Electron. 70 (Juli 2019) 286–291, https://doi.org/10.1016/j.orgel.2019.04.033.

[8] W. Song, T. Kim, J.Y. Lee, Y. Lee, H. Jeong, Investigation of degradation mechanism of phosphorescent and thermally activated delayed fluorescent organic light-emitting diodes through doping concentration dependence of lifetime, Bd. J. Ind. Eng. Chem. 68 (Dez. 2018) 350–354, https://doi.org/10.1016/j.jiec.2018.08.006.

[9] Y.K. Moon, H.J. Jang, S. Hwang, S. Kang, S. Kim, J. Oh, S. Lee, D. Kim, J.Y. Lee, Y. You, Modeling electron-transfer degradation of organic light-emitting devices, Bd. Adv. Mater. 33 (12) (2021), 2003832 https://doi.org/10.1002/adma.202003832.

[10] H. Yu, Y. Zhang, Y.J. Cho, H. Aziz, Exciton-induced degradation of carbazole-based host materials and its role in the electroluminescence spectral changes in phosphorescent organic light emitting devices with electrical aging, Bd. ACS Appl. Mater. Interfaces 9 (16) (Apr. 2017) 14145–14152, https://doi.org/10.1021/acsami.7b01432.

[11] X. Zheng, F. Cao, C. Wang, T. Tsuboi, Y. Zhu, Q. Ai, C. Deng, D. Wang, L. Su, Z. Liu, Q. Zhang, Expanding the hole delocalization range in excited molecules for stable organic light-emitting diodes employing thermally activated delayed fluorescence, Bd. J. Mater. Chem. C 8 (29) (2020) 10021–10030, https://doi.org/10.1039/D0TC01897J.

[12] M. Tanaka, H. Noda, H. Nakanotani, C. Adachi, Effect of carrier balance on device degradation of organic light-emitting diodes based on thermally activated delayed fluorescence emitters, Bd. Adv. Electron. Mater. 5 (5) (2019), 1800708 https://doi.org/10.1002/aelm.201800708.

[13] W. Song, J.Y. Lee, Design strategy of exciplex host for extended operational lifetime, Bd. Org. Electron. 48 (Sep. 2017) 285–290, https://doi.org/10.1016/j.orgel.2017.06.024.

[14] Q. Wang, H. Aziz, Exciton–Polaron-induced aggregation of organic electroluminescent materials: a major degradation mechanism in wide-bandgap phosphorescent and fluorescent organic light-emitting devices, Bd. Adv. Opt. Mater. 3 (7) (2015) 967–975, https://doi.org/10.1002/adom.201400640.

[15] J.-M. Kim, C.-H. Lee, J.-J. Kim, Mobility balance in the light-emitting layer governs the polaron accumulation and operational stability of organic light-emitting diodes, Bd. Appl. Phys. Lett. 111 (20) (Nov. 2017), 203301 https://doi.org/10.1063/1.5004623.

[16] H.Z. Siboni, H. Aziz, Causes of driving voltage rise in phosphorescent organic light emitting devices during prolonged electrical driving, Bd. Appl. Phys. Lett. 101 (17) (2012), 173502 https://doi.org/10.1063/1.4764021. Okt

[17] D.Y. Kondakov, J.R. Sandifer, C.W. Tang, R.H. Young, Nonradiative recombination centers and electrical aging of organic light-emitting diodes: direct connection between accumulation of trapped charge and luminance loss, Bd. J. Appl. Phys. 93 (2) (Jan. 2003) 1108–1119, https://doi.org/10.1063/1.1531231.

[18] Q. Wang, H. Aziz, Degradation of organic/organic interfaces in organic light-emitting devices due to polaron–exciton interactions, Bd. ACS Appl. Mater. Interfaces 5 (17) (Sep. 2013) 8733–8739, https://doi.org/10.1021/am402537j.

[19] T.D. Schmidt, L. Jäger, Y. Noguchi, H. Ishii, W. Brütting, Analyzing degradation effects of organic light-emitting diodes via transient optical and electrical measurements, Bd. J. Appl. Phys 117 (21) (Juni 2015), 215502 https://doi.org/10.1063/1.4921829.

[20] B. Sim, J.S. Kim, H. Bae, S. Nam, E. Kwon, J.W. Kim, H.-Y. Cho, S. Kim, J.-J. Kim, Comprehensive model of the degradation of organic light-emitting diodes and application for efficient, stable blue phosphorescent devices with reduced influence of polarons, Bd. Phys. Rev. Appl. 14 (Nr. 2) (Aug. 2020) https://doi.org/10.1103/PhysRevApplied.14.024002. S. 024002

[21] M.T. Neukom, S. Züfle, B. Ruhstaller, Reliable extraction of organic solar cell parameters by combining steady-state and transient techniques, Bd. Org. Electron. 13 (12) (Dez. 2012) 2910–2916, https://doi.org/10.1016/j.orgel.2012.09.008.

[22] J.-H. Lee, H. Shin, J.-M. Kim, K.-H. Kim, J.-J. Kim, Exciplex-forming Co-Host-Based red phosphorescent organic light-emitting diodes with long operational stability and high efficiency, Bd. ACS Appl. Mater. Interfaces 9 (4) (Feb. 2017) 3277–3281, https://doi.org/10.1021/acsami.6b14438.

[23] Fluxim, Provider of device simulation software setfos and characterization platform paios, phelos, litos and litos lite. https://www.fluxim.com.

[24] G. Juška, K. Arlauskas, M. Viliūnas, J. Kočka, Extraction current transients: new method of study of charge transport in microcrystalline silicon, Bd. Phys. Rev. Lett. 84 (21) (Mai 2000) 4946–4949, https://doi.org/10.1103/PhysRevLett.84.4946.

[25] S. Züfle, S. Altazin, A. Hofmann, L. Jäger, M.T. Neukom, T.D. Schmidt, W. Brütting, B. Ruhstaller, The use of charge extraction by linearly increasing voltage in polar organic light-emitting diodes, Bd. J. Appl. Phys. 121 (17) (Mai 2017), 175501 https://doi.org/10.1063/1.4982903.

[26] M. Regnat, K.P. Pernstich, B. Ruhstaller, Influence of the bias-dependent emission zone on exciton quenching and OLED efficiency, Bd. Org. Electron. 70 (Juli 2019) 219–226, https://doi.org/10.1016/j.orgel.2019.04.027.

[27] S. Jenatsch, S. Züfle, B. Blülle, B. Ruhstaller, Combining steady-state with frequency and time domain data to quantitatively analyze charge transport in organic light-emitting diodes, Bd. J. Appl. Phys. 127 (Jan. 2020) https://doi.org/10.1063/1.5132599. Nr. 3, S. 031102

[28] B. Ruhstaller, E. Knapp, B. Perucco, N. Reinke, D. Rezzonico, F. Müller, Advanced numerical simulation of organic light-emitting devices, in: Oleg Sergiyenko (Ed.), Optoelectronic Devices and Properties, 2011, ISBN 978-953-307-204-3, 10.5772/14626.

[29] B. Perucco, N.A. Reinke, D. Rezzonico, E. Knapp, S. Harkema, B. Ruhstaller, On the exciton profile in OLEDs-seamless optical and electrical modeling, Bd. Org. Electron. 13 (10) (2012) 1827–1835, https://doi.org/10.1016/j.orgel.2012.05.053. Okt

[30] B. Ruhstaller, S.A. Carter, S. Barth, H. Riel, W. Riess, J.C. Scott, Transient and steady-state behavior of space charges in multilayer organic light-emitting diodes, Bd. J. Appl. Phys. 89 (8) (Apr. 2001) 4575–4586, https://doi.org/10.1063/1.1352027.

[31] M. Regnat, K.P. Pernstich, K.-H. Kim, J.-J. Kim, F. Nüesch, B. Ruhstaller, Routes for efficiency enhancement in fluorescent TADF exciplex host OLEDs gained from an electro-optical device model, Adv. Electron. Mater. (2019), 1900804, https://doi.org/10.1002/aelm.201900804. Bd. n/a, Nr. n/a, S.

[32] Y. Noguchi, W. Brütting, H. Ishii, Spontaneous orientation polarization in organic light-emitting diodes, Bd. Jpn. J. Appl. Phys. 58 (Mai 2019) https://doi.org/10.7567/1347-4065/ab0de8. Nr. SF, S. SF0801

[33] M. Regnat, K.P. Pernstich, S. Züfle, B. Ruhstaller, Analysis of the bias-dependent split emission zone in phosphorescent OLEDs, *ACS Appl. Mater. Interfaces*, Bd. 10 (37) (Sep. 2018) 31552–31559, https://doi.org/10.1021/acsami.8b09595.

[34] B. Perucco, N.A. Reinke, D. Rezzonico, M. Moos, B. Ruhstaller, Analysis of the emission profile in organic light-emitting devices, *Opt. Express*, Bd. 18 (102,) (Juni 2010), https://doi.org/10.1364/OE.18.00A246. A246–A260.

[35] Y. Noguchi, H. Lim, T. Isoshima, E. Ito, M. Hara, W.W. Chin, J.W. Han, H. Kinjo, Y. Ozawa, Y. Nakayama, H. Ishii, Influence of the direction of spontaneous orientation polarization on the charge injection properties of organic light-emitting diodes, Bd. Appl. Phys. Lett. 102 (20) (Mai 2013), 203306 https://doi.org/10.1063/1.4807797.

[36] Y.-S. Park, S. Lee, K.-H. Kim, S.-Y. Kim, J.-H. Lee, J.-J. Kim, Exciplex-forming Co-host for organic light-emitting diodes with ultimate efficiency, Bd. Adv. Funct. Mater. 23 (39) (2013) 4914–4920, https://doi.org/10.1002/adfm.201300547.

[37] H. Shin, S. Lee, K.-H. Kim, C.-K. Moon, S.-J. Yoo, J.-H. Lee, J.-J. Kim, Blue phosphorescent organic light-emitting diodes using an exciplex forming Co-host with the external quantum efficiency of theoretical limit, Bd. Adv. Mater. 26 (27) (Juli 2014) 4730–4734, https://doi.org/10.1002/adma.201400955.

[38] B. Zhao, T. Zhang, B. Chu, W. Li, Z. Su, H. Wu, X. Yan, F. Jin, Y. Gao, C. Liu, Highly efficient red OLEDs using DCJTB as the dopant and delayed fluorescent exciplex as the host, Bd. Sci. Rep. 5 (Mai 2015) https://doi.org/10.1038/srep10697. S. srep.10697

[39] S. Züfle, S. Altazin, A. Hofmann, L. Jäger, M.T. Neukom, W. Brütting, B. Ruhstaller, Determination of charge transport activation energy and injection barrier in organic semiconductor devices, Bd. J. Appl. Phys. 122 (11) (Sep. 2017), 115502 https://doi.org/10.1063/1.4992041.

[40] T. Morgenstern, M. Schmid, A. Hofmann, M. Bierling, L. Jäger, W. Brütting, Correlating optical and electrical dipole moments to pinpoint phosphorescent dye alignment in organic light-emitting diodes, Bd. ACS Appl. Mater. Interfaces 10 (37) (Sep. 2018) 31541–31551, https://doi.org/10.1021/acsami.8b08963.

[41] J. Staudigel, M. Stößel, F. Steuber, J. Simmerer, A quantitative numerical model of multilayer vapor-deposited organic light emitting diodes, Bd. J. Appl. Phys. 86 (7) (Sep. 1999) 3895–3910, https://doi.org/10.1063/1.371306.

[42] D. Kondakov, Chemical transformations of common hole transport materials in operating OLED devices, in: Organic Light Emitting Materials and Devices XII, Sep. 2008, https://doi.org/10.1117/12.796824. Bd. 7051, S. 70510I.

[43] S.-C. Dong, L. Xu, C.W. Tang, Chemical degradation mechanism of TAPC as hole transport layer in blue phosphorescent OLED, Bd. Org. Electron. 42 (März 2017) 379–386, https://doi.org/10.1016/j.orgel.2016.11.041.

[44] D.Y. Kondakov, Role of chemical reactions of arylamine hole transport materials in operational degradation of organic light-emitting diodes, Bd. J. Appl. Phys. 104 (2008) https://doi.org/10.1063/1.3006890. Nr. 8, S. 084520, Okt

[45] W. Song, J.Y. Lee, T. Kim, Y. Lee, H. Jeong, Comprehensive understanding of degradation mechanism of high efficiency blue organic light-emitting diodes at the interface by hole and electron transport layer, Bd. Org. Electron. 57 (Juni 2018) 158–164, https://doi.org/10.1016/j.orgel.2018.03.010.

[46] C. Li, L. Duan, H. Li, Y. Qiu, Universal trap effect in carrier transport of disordered organic semiconductors: transition from shallow trapping to deep trapping, Bd. J. Phys. Chem. C 118 (20) (Mai 2014) 10651–10660, https://doi.org/10.1021/jp5022906.

[47] E. Knapp, B. Ruhstaller, The role of shallow traps in dynamic characterization of organic semiconductor devices, Bd. J. Appl. Phys. 112 (2) (Juli 2012) https://doi.org/10.1063/1.4739303. S. 024519

[48] S. Scholz, D. Kondakov, B. Lüssem, K. Leo, Degradation mechanisms and reactions in organic light-emitting devices, Bd. Chem. Rev. 115 (16) (Aug. 2015) 8449–8503, https://doi.org/10.1021/cr400704v.